

Fullerene Derivative-Doped Zinc Oxide Nanofilm as the Cathode of Inverted Polymer Solar Cells with Low-Bandgap Polymer (PTB7-Th) for High Performance

Sih-Hao Liao, Hong-Jyun Jhuo, Yu-Shan Cheng, and Show-An Chen*

Bulk-heterojunction (BHJ) polymer solar cells (PSCs)^[1] with an active layer composed of a conjugated polymer as the donor and a fullerene derivative as the acceptor have attracted great attention because of their ease of fabrication, promising flexibility, and capability for large-scale and low-cost production. Poly(3-hexylthiophene) (P3HT) with high regioregularity and [6,6]-phenyl-C₆₁-butyric acid methyl ester (PC₆₁BM) are the most representative conjugated polymer donor material and acceptor material, respectively. PSCs based on these two materials can reach power conversion efficiencies (PCEs) of 4–5%.^[2] There are two types of device structure of BHJ PSCs: conventional PSCs (c-PSCs) and inverted PSCs (i-PSCs). For a c-PSC, an active layer composed of polymer donor and acceptor material is sandwiched between transparent conducting indium tin oxide (ITO), usually coated with poly(3,4-ethylenedioxythiophene) poly(styrenesulfonate) (PEDOT:PSS), as the anode and a low-work-function metal electrode as the cathode. However, prolonged exposure of this kind of device to air can lead to an oxidation of the air-sensitive metal cathode, resulting in degradation of the PSC.^[3] In order to alleviate this problem, an approach involving an inversion of the device architecture (i-PSC) is employed, in which a less air-sensitive high-work-function metal (Ag, Au) is used as the back, hole-collecting electrode and ZnO or TiO_x is used as the electron-collecting interlayer between ITO and the active layer.^[4–6] However, the inorganic electron-collecting interlayer could have poor interfacial contact with the organic active layer, resulting in poor electron extraction,^[7] and thus interface modification becomes an important issue for improving electron extraction in i-PSCs.

To reach high PCE, one has to use a low-bandgap polymer as the donor with high highest occupied molecular orbital (HOMO) energy level to harvest more sunlight (and thus higher short circuit current J_{sc}) and higher open circuit voltage V_{oc} , and use interlayers or electrode modification for effective collection of charges. Among the reported effective low-bandgap polymers, the series of copolymers composed of the two basic fused-ring comonomer units benzodithiophene (BDT) and thieno[3,4-b]thiophene (TT) are of particular interest since they

S.-H. Liao, H.-J. Jhuo, Y.-S. Cheng, Prof. S.-A. Chen
Chemical Engineering Department
and Frontier Research Center on Fundamental
and Applied Sciences of Matters
National Tsing-Hua University
Hsinchu 30013, Taiwan, ROC
E-mail: sachen@che.nthu.edu.tw

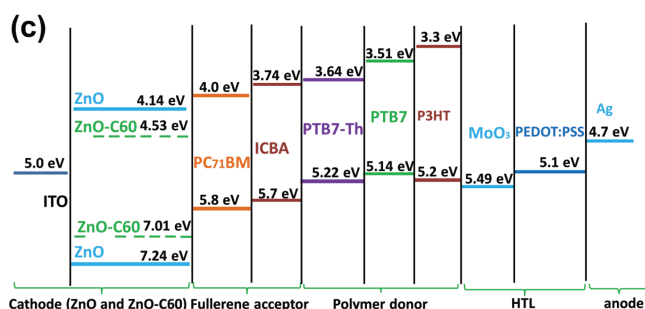
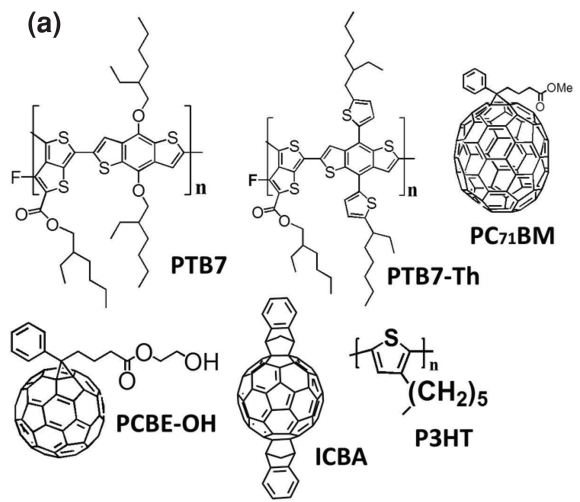
DOI: 10.1002/adma.201301476



offer very high PCE resulting from higher J_{sc} and V_{oc} . Modifications to these two basic units were made by incorporating the electron-donating 2-ethylhexyloxy group as side chains into the BDT unit and electron-withdrawing fluorine atoms into the TT unit with the *n*-octyl carboxylate group as a side chain, giving PCE = 6.1%^[8] in c-PSC, in which the fluorine substituent is to increase its HOMO level. This PCE is significantly higher than that without F-substitution (4.1%). Further fine tuning of the chemical structure above by replacing the carboxylic ester group in the F-substituted TT unit with an *n*-heptylacyl group (designated as PBDTTT-CF)^[9] or a 2-ethylhexyl carboxylate group (designated as PTB7)^[10] increased PCE to 7.73% and 7.4%, respectively. Another way the structure of the PBDTTT copolymer was modified was to tune the BDT unit by incorporation of alkyl-thienyl groups as its side chains, while the TT unit was only modified with an alkylcarbonyl group, without F-substitution (designated as PBDTTT-C-T);^[11] the PCE of the c-PSC was then 7.59%, close to the case with modification of the TT unit by F-substitution. The modifications to the BDT unit or TT unit above provided very similar device performance in terms of J_{sc} , V_{oc} , and PCE.

In order to improve electron and hole collection for further PCE enhancement, interlayers have been inserted between the electrodes. In c-PSCs, the alcohol-soluble electron transport layer (ETL) having optical spacer functionality based on polyfluorene grafted with a K+-intercalated crown ether (PFCN₆:K<+>)^[12] used with the donor:acceptor pair P3HT:indene-C₆₀ bisadduct (ICBA) enhanced the PCE from 5.78% to 7.5%, while the alcohol:acetic acid (99.8:0.2, v/v)-soluble polyfluorene grafted with the polar functional group *N,N*-dimethylamino (PFN) applied for the pair PTB7:PC₇₁BM increased PCE from 7.13% to 8.37%.^[13] Meanwhile, in i-PSCs, the insertion of a self-assembled monolayer of fullerene derivatives^[14] on a ZnO surface raised PCE for the P3HT:PC₆₁BM pair from 3.47% to 4.4%, while applying the crosslinkable fullerene derivative [6,6]-phenyl-C₆₁-butyric styryl dendron ester (PCBSD)^[7] to the P3HT:PC₆₁BM pair changed PCE from 3.5% to 4.4%, and to the P3HT:ICBA pair, from 4.8% to 6.2%.^[15] Applying a crosslinked fullerene as a nanorod array on ZnO for the P3HT:ICBA pair gave PCE = 7.3%,^[16] and applying PFN as interlayer on the ITO cathode surface for the pair PTB7:PC₇₁BM gave PCE up to 9.21%.^[17]

Here we propose a novel PBDTTT-type low-bandgap polymer as the donor that combines the advantage of incorporating the 2-ethylhexyl-thienyl group into the BDT unit (BDT-T) in PTB7 to improve the coplanarity of the main chain so that the absorption band can be extended to longer wavelengths by 25 nm,



Scheme 1. a) Chemical structures of the materials used for device fabrication. b) Reaction scheme for synthesis of ZnO-C60. c) Energy level diagram for ZnO-C60 determined from UPS, UV-vis, and CV results, and taken from the literature for all the other materials: P3HT and PEDOT,^[12] PC₇₁BM,^[18] ICBA,^[19] and MoO₃.^[20]

along with increased absorption coefficient, with the advantage of retaining the fluorine-substituted TT unit (F-TT) with the 2-ethylhexyl carboxylate group for higher HOMO level. This novel copolymer (designated as PTB7-Th) as the donor (**Scheme 1a**), along with PC₇₁BM as the acceptor, is used as the active layer of the present i-PSC. For effective collection of electrons, we further propose a fullerene derivative (PCBE-OH)-doped ZnO nanometer-thick film (40 nm) as the cathode (designated as ZnO-C60, Scheme 1b). The doping creates a negative

polaron state of ZnO 0.39 eV below its lowest unoccupied molecular orbital (LUMO) level and improves the bulk electron conductivity. Yet the interface of ZnO-C60 with the active layer is rich in the fullerene derivative. The resulting device with the active layer PTB7-Th:PC₇₁BM and the cathode ZnO-C60 gives PCE = 9.35%, which is higher than that obtained by replacing PTB7-Th with PTB7 (8.21%); corresponding devices with pristine ZnO give PCE = 7.64% and 6.65%, respectively. The PCE of 9.35% is one of the best results that have been reported so far.

The copolymer PTB7-Th was synthesized through a Stille coupling reaction between the bis(trimethyltin) BDT-T monomer and the dibromide F-TT. The detailed synthesis procedures for the monomers and polymers are described in the Supporting Information.

The UV-vis absorption spectra of PTB7 and PTB7-Th films and their blends with PC₇₁BM as films formed by spin-casting from the solutions in chlorobenzene (CB, for the polymers) and CB/1,8-diiodooctane (CB/DIO, for the blends; 97:3, v/v), respectively, are shown in Figures 1a,b. The range of the absorption band of PTB7-Th (500–785 nm) is extended toward longer wavelengths by 25 nm relative to that of PTB7 (500–760 nm), yet the former has slightly higher absorption coefficient than the latter. The optical bandgap determined from the absorption onset for PTB7 (1.63 eV) is higher by 0.05 eV than that of PTB7-Th (1.58 eV), which can be attributed to the enhanced intermolecular π - π stacking by the incorporation of two thiophene units as side chains in PTB7-Th.^[11,21] For the blend films (Figure 1b), as in the case of polymer alone, PTB7-Th:PC₇₁BM gives a wider absorption range toward longer wavelength and slightly higher absorption coefficient relative to that for PTB7:PC₇₁BM.

To confirm that PTB7-Th blended with PC₇₁BM provides better intermolecular π - π stacking than PTB7 blended with PC₇₁BM, thin-film grazing incidence wide-angle X-ray scattering (GIWAXS) measurements were performed on them; the results are given in Figure S10 (Supporting Information). Both the in-plane and out-of-plane scattering patterns are similar in character for both blends, indicating that the intermolecular π - π stacking domains are randomly distributed. Their lamellar spacings are 17.95 Å ($q = 0.35 \text{ \AA}^{-1}$) and 17 Å ($q = 0.36 \text{ \AA}^{-1}$) and their π - π stacking distances between the backbones are 3.22 Å ($q = 1.95 \text{ \AA}^{-1}$) and 3.47 Å ($q = 1.81 \text{ \AA}^{-1}$), respectively. The PTB7-Th:PC₇₁BM blend has a peak at 0.35 Å⁻¹ with higher and sharper intensity (600 counts), from $q = 0.2$ to 0.45 Å⁻¹, than the peak at 0.36 Å⁻¹ of the PTB7:PC₇₁BM blend (400 counts) from $q = 0.2$ to 0.6 Å⁻¹. These results indicate that PTB7-Th in the blend has high co-planarity of the main chain as a result of the introduction of 2-ethylhexyl-thienyl groups into benzodithiophene.

From the density functional theory (DFT) calculation, it can be observed that at the side chains of the monomers, the HOMO level of PTB7-Th is more delocalized than that of PTB7, as shown in Figures S1a,b (Supporting Information). This difference can be ascribed to the enhanced conjugation that extends the absorption band toward longer wavelength. The DFT calculation also gives the HOMO energy levels of the monomers of PTB7 and PTB7-Th as 5.03 and 5.13 eV and their corresponding LUMOs as 2.17 and 2.23 eV, respectively. The

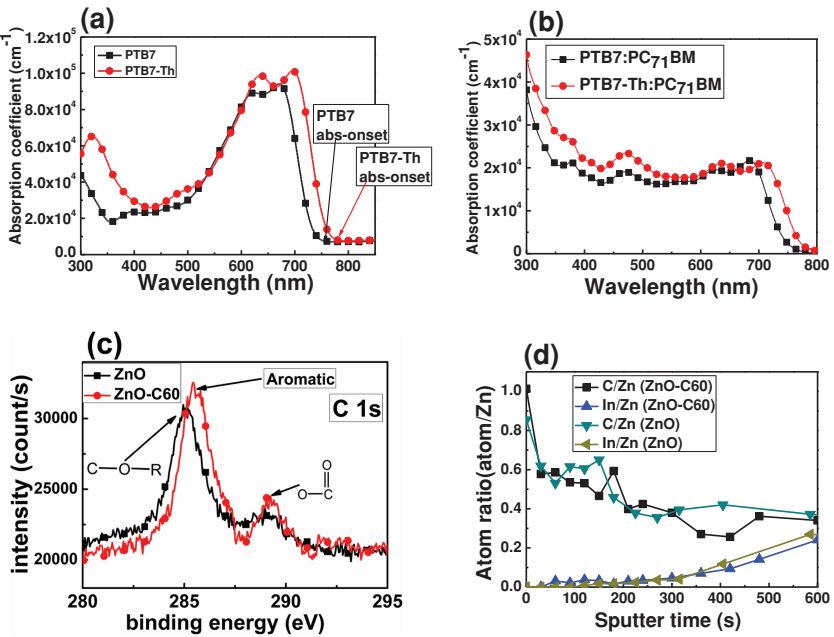


Figure 1. a,b) UV-visible absorption spectra of thin films of PTB7 and PTB7-Th (a), and PTB7 and PTB7-Th blend with PC₇₁BM (b). c,d) XPS analysis on ITO/ZnO and ITO/ZnO-C60: c) carbon C 1s BE and d) depth profiles of the atom ratios C/Zn and In/Zn in ZnO and ZnO-C60.

results of cyclic voltammetry (CV) measurements in Figure S1c and Table S1 (both in the Supporting Information) also show the same trend: that PTB7-Th also has a higher HOMO level (5.22 eV) — by 0.08 eV — than PTB7 (5.14 eV). The higher HOMO level of PTB7-Th is expected to give a higher V_{oc} in i-PSC, as will be revealed below.

ZnO-C60 and pristine ZnO nanofilms (40 nm thick) were prepared by spin-casting either a solution of the mixture of 0.5 wt% PCBE-OH and 99.5 wt% zinc acetate ($\text{Zn}(\text{Ac})_2$) in a mixture of 2-methoxyethanol and ethanolamine, or a solution without PCBE-OH, also in a mixture of 2-methoxyethanol and ethanolamine, on top of ITO and then sintering at 180 °C in air as shown in Scheme 1b. The procedure for preparation of the ZnO nanofilm was in accordance with that reported previously^[22] but the ethanolamine weight ratio used is less by 10 wt% (see details in the Supporting Information). The resulting ZnO-C60 and pristine ZnO films on ITO were then rinsed with a solvent of PCBE-OH, carbon disulfide (CS_2), to remove the nonbonding residual PCBE-OH on the surface, and subsequently dried for further characterization by contact angle measurement, X-ray and ultraviolet photoelectron spectroscopy (XPS and UPS), ultraviolet-visible absorption spectroscopy (UV-vis), and charge transport measurement.

We measured the contact angles of the nanofilms with deionized (DI) water (Figure S2, Supporting Information) and found that the ZnO-C60 surface is more hydrophobic than the pristine ZnO (designated as ZnO) surface, since the contact angle changes from 28° for ZnO to 47° for ZnO-C60. Taking into consideration that the contact angle of C₆₀ self-assembled monolayers (C₆₀-SAMs) ranges from 40° to 60°,^[14] we can infer that the surface of ZnO-C60 is mostly covered with the fullerene derivative. We also prepared samples of ZnO and ZnO-C60 on ITO glass before and after rinsing with CS_2 for

atomic force microscopy (AFM) morphology measurements, as shown in Figure S11 (Supporting Information). Before and after CS_2 rinsing (which removes residual PCBE-OH and impurities on the surface), the ZnO films show similar lattice grain morphology, while the ZnO-C60 films show destroyed lattice grain morphology. The rinsed ZnO-C60 exhibited less-aligned grains on the surface compared to ZnO-C60 before rinsing. Note that the morphology of the present ZnO is different from that in the previous report^[22] since the amount of ethanolamine used is less.

XPS measurements for binding energy (BE) spectra of various types of carbon on the surface and the element content depth profiles for ZnO-C60 and ZnO nanofilms are shown in Figures 1c,d. The C 1s BE spectrum of ZnO in Figure 1c shows two characteristic peaks: the one located at lower BE (285 eV) is from C-OR^[23] ($\text{R} = \text{C}_2\text{H}_5$ group) and the other, at higher BE (288.5 eV), is from the carbonyl^[23] group. In ZnO-C60, there are also two characteristic peaks: one at lower BE (285.7 eV, which is higher than that of C-OR

by 0.7 eV) and the other at higher BE (288.7 eV), which is from the carbonyl^[23] group. The BE spectra of C60 and PC₆₁BM were found to contain the same main peak (C 1s), at 285.2 eV, contributed by the aromatic carbon,^[24] while for PCBM there were also two smaller peaks: at 286.9 eV, contributed by the carbon of the methyl group, and at 289.8 eV, associated with the carbonyl group.^[24] Thus, the major C 1s peak at 285.7 eV of C 1s can be attributed to aromatic carbons from fullerene derivatives (PCBE-OH) in ZnO-C60, which is in agreement with the contact angle result above. The shift to higher BE by 0.5 eV could be attributed to the electron transfer to ZnO by the doping. Since the fullerene content in the bulk solid of the precursor is only 0.5 wt% and the surface is fullerene rich, it is necessary to examine the atomic content profiles along the ZnO-C60 layer. It can be clearly observed from Figure 1d that, at the surface, the C/Zn atomic ratio of ZnO-C60 (1.01) is higher than that of ZnO (0.85) by 0.16 (or a factor of 1.19), which is also higher than that of the unsintered homogeneous case (0.07) by a factor of 2 (because the C/Zn of unsintered Zn-C60 is calculated to be 2.06 and that of ZnO is 1.99). This indicates that the surface of ZnO-C60 is rich in fullerene derivative. In contrast, the In/Zn atom ratio profiles in both cases are very close and, for a sputtering time less than about 300 s, nearly zero, which would indicate that a sputtering time of 300s is equivalent to the thickness of both coated layers, 40 nm. The C/Zn atom ratio profiles of ZnO-C60 (1.01) and ZnO (0.85) are reduced rapidly to 0.59 and 0.61, respectively, at a sputtering time of 40 s, indicating that the fullerene derivative in ZnO-C60 is mainly located in a region within 5.3 nm of the interface, as estimated by assuming a linear variation of sputtering time with thickness.

Further analysis of XPS results on BE for zinc, oxygen, and carbon atoms at the surfaces of ZnO and ZnO-C60 are given below to reveal that ZnO in ZnO-C60 is doped. The BE spectra

of C 1s, O 1s, Zn 2p_{1/2}, and Zn 2p_{3/2} of ZnO and ZnO-C60 are shown in Figure S3 (Supporting Information). As can be seen, the BE peaks of Zn 2p_{1/2} (1023.44 eV) and 2p_{3/2} (1046.49 eV) of ZnO-C60 are both higher by 0.7 eV than those of ZnO (Zn 2p_{1/2} (1022.74 eV) and 2p_{3/2} (1045.79 eV)). We infer that the electronic states of ZnO in ZnO-C60 are similar to those in Al-doped ZnO (N-type),^[25] in which its Zn 2p_{1/2} and 2p_{3/2} BE both shift to higher energy by 0.9 eV^[25] relative to ZnO. The BE peaks of O 1s in the ZnO are 532.5 eV and 531.5 eV for O-H^[26] and Zn-O,^[26] respectively, while those in ZnO-C60 give only one peak, at 530.8 eV, which can be attributed to O in ZnO by shifting to lower energy by 0.7 eV relative to the pristine ZnO. The signal of BE O 1s of 532.5 eV (OH) disappears in ZnO-C60, indicating that the defect with O-H on the ZnO surface is eliminated after the doping, which would also contribute partially to the enhancement in electron extraction efficiency.^[22]

To investigate whether ZnO in the bulk of ZnO-C60 is also doped by PCBE-OH as on its surface, we examined the UV-vis spectra (Figure S4a, Supporting Information) of the ZnO-C60 and ZnO and found that the former shows additional absorption in the range 400–500 nm, indicating the occurrence of doping by which additional electronic states are generated in the bandgap.^[27] We then turn to determining the electronic energy levels (HOMO and LUMO levels of ZnO and ZnO-C60) using UPS (Figure S4b and Table S2, see details in Text S3, Supporting Information). ZnO-C60's HOMO level (7.01 eV) is lowered by 0.23 eV relative to ZnO's HOMO level (7.24 eV). Note that such change is due to the n-doping rather than interfacial dipole as evidenced by the generation of additional optical absorption indicated above. The LUMO levels of ZnO and ZnO-C60 can then be determined by including their optical bandgaps as follows: LUMO level = HOMO level – optical bandgap, where the optical bandgaps of ZnO and ZnO-C60 are 3.10 and 2.48 eV, respectively as determined from the optical absorption spectra in Figure S4a (Supporting Information). The resulting LUMO levels are 4.14 (ZnO) and 4.53 eV (ZnO-C60). The doping creates a new transport pathway for electrons. Furthermore the higher content of fullerene at the surface offers a better contact to the fullerene derivative in the active layer to facilitate electron collection. The energy levels so determined along with those of the other materials are summarized in Scheme 1c.

In ZnO-C60, the created electronic states would allow an improvement in conductivity relative to ZnO as expected. We measured electron mobility (μ) across the film by applying single-carrier space charge limited conduction (SCLC) on the electron-only device ITO/Al/ZnO or ZnO-C60/Al, and the results are shown in Figure S5 and Table S3 (Supporting Information). The electron mobility of ZnO-C60 is significant higher than that of ZnO by a factor of 50, from 4.9×10^{-5} to $2.7 \times 10^{-3} \text{ cm}^2 \text{ V}^{-1} \text{ s}^{-1}$ (the value for ZnO is close to the reported value $1.8 \times 10^{-4} \text{ cm}^2 \text{ V}^{-1} \text{ s}^{-1}$).^[28] Furthermore, we also measured the surface conductivities for ZnO and ZnO-C60 using the four-probe method and found that the surface conductivity increases by a factor of 73 from 0.015 (ZnO) to 1.09 (ZnO-C60) S cm⁻¹ (the ZnO value is lower than the reported value 0.187 S cm⁻¹ using the same method)^[29] (Table S4, Supporting Information).

We then applied ZnO-C60 coated on ITO as the cathode for i-PSCs with the device structure ITO/ZnO or ZnO-C60/active

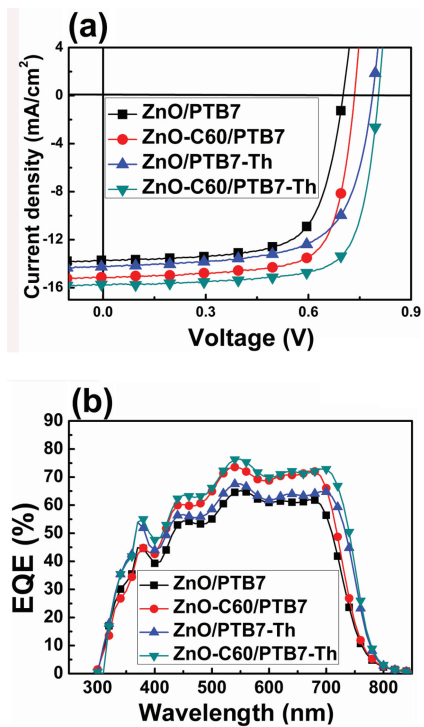


Figure 2. a,b) Performance of i-PSC under simulated 100 mW cm⁻² AM 1.5G illumination. J-V curves (a) and EQE spectra (b) of the devices ITO/ZnO or ZnO-C60 (40 nm)/PTB7:PC₇₁BM or PTB7-Th:PC₇₁BM (1:1.5 w/w, 100 nm)/MoO₃ (10 nm)/Ag (100 nm).

layer/MoO₃/Ag under simulated 100 mW cm⁻² AM 1.5G illumination; their performance characteristic values are listed in **Figure 2a** and **Table 1**. For the devices with the active layer PTB7:PC₇₁BM, use of ZnO-C60 as the cathode gives remarkably enhanced performance relative to that with ZnO, as the PCE increases from 6.65% to 8.21%. For the devices with the presented novel low-bandgap polymer PTB7-Th as the donor and PC₇₁BM as the acceptor, use of ZnO-C60 also gives remarkably increased performance relative to that with ZnO, as the PCE increases from 7.64% to 9.35%; all three of the corresponding parameters (V_{oc} , the short-circuit current density J_{sc} , and the fill factor FF) were improved, from 0.79 V, 14.02 mA cm⁻², and 69.1%, to 0.80 V, 15.73 mA cm⁻², and 74.3%, respectively. Besides PTB7 and PTB7-Th, we also investigated another active layer, P3HT:ICBA. For the device ITO/ZnO or ZnO-C60/active layer/PEDOT: PSS/Ag, their J-V curves are given in Figure S6

Table 1. Photovoltaic performance of i-PSCs based on PC₇₁BM with the device structure ITO/ZnO or ZnO-C60 (40 nm)/PTB7:PC₇₁BM or PTB7-Th:PC₇₁BM (1:1.5 w/w, 100 nm)/MoO₃ (10 nm)/Ag (100 nm).

Cathode	Donor	V_{oc} [V]	J_{sc} [mA cm ⁻²]	FF [%]	PCE [%]
ZnO	PTB7	0.70	13.75	69.0	6.65
ZnO-C60	PTB7	0.73	15.41	73.0	8.21
ZnO	PTB7-Th	0.79	14.02	69.1	7.64
ZnO-C60	PTB7-Th	0.80	15.73	74.3	9.35

and their performance parameters are listed in Table S5 (Supporting Information). The use of ZnO-C60 as the cathode gives significantly improved performance relative to that with ZnO, as the PCE increases from 5.29% to 6.60%.

According to the characterization of ZnO-C60 above, the improvement in PCE can be attributed mainly to the additional transport pathway for electrons created by the high coverage of the fullerene derivatives on the ZnO surface (Schemes 1b,c) and to the promoted electron conduction on the surface and in the bulk of ZnO-C60. Therefore the chance for electron/hole recombination at the interface is reduced by cutting off the chance of direct contact of polymer with the ZnO, facilitating a more effective collection of electrons from the bulk. PTB7-Th provides higher PCE than PTB7 by about 1% for both ZnO-C60 and ZnO and the physics behind this is given above; the corresponding V_{oc} of PTB7-Th (0.80 V) is only higher than that of PTB7 (0.73 V) by 0.07 V, which correlates well with the increase in HOMO level by 0.08 V (Table 1). Therefore the improvement in PCE from 8.21% (PTB7) to 9.35% (PTB7-Th) results mainly from the promotion of intermolecular coplanarity by introducing two thiophene units to the BDT unit. Overall, this work proposes modifications of PTB7 in the active layer and ZnO cathode, which lead to a great improvement in PCE from 6.65% to 9.35%.

External quantum efficiency (EQE) measurements for the devices with PTB7 and PTB7-Th show overall enhancement in the entire absorption range when ZnO-C60 is used instead of ZnO as the cathode (Figure 2b), which implies that the increase of current density results from more-efficient electron collection by the ZnO-C60 than ZnO. With ZnO-C60 cathode for both devices with PTB7 and PTB7-Th, the EQEs from 500 to 700 nm are in the range 65%–75%, which are much higher than those with ZnO (55%–65%); at the same time, those of the latter polymer (PTB7-Th) are slightly higher than those of PTB7 in both types of cathode. However, the EQEs in the absorption range 700–750 nm of the PTB7-Th device are significantly higher than those of the PTB7 device for both types of cathode, which is due to the additional absorption provided by PTB7-Th. The additional electron collection enhancement can also be manifested by the calculations of series resistance (R_s) and shunt resistance (R_{sh}) from reciprocals of the slopes of the $J-V$ curves at $I=0$ and $V=0$.^[12] For the PTB7 devices with ZnO and ZnO-C60, a significant drop in R_s from 15.13 to 4.16 $\Omega \text{ cm}^2$, and a drastic rise in R_{sh} from 957 to 1378 $\Omega \text{ cm}^2$, respectively (Table S6, Supporting Information) are found. For the PTB7-Th devices with ZnO and ZnO-C60, a significant drop in R_s from 13.46 to 2.78 $\Omega \text{ cm}^2$, and a drastic rise in R_{sh} from 1001 to 1451 $\Omega \text{ cm}^2$, respectively (Table S6) are found. Indeed, the electrical leakage for the devices with ZnO-C60 is considerably suppressed (Figure S7, Supporting Information). In addition, we also measured R_s from impedance in the dark under a bias of 0.8 V. For the same devices of PTB7 with ZnO and ZnO-C60, a drop in R_s from 31 to 26 $\Omega \text{ cm}^2$ (Figure S8 and Table S7, Supporting Information) is found; and for the same devices of PTB7-Th with ZnO and ZnO-C60, a drop in R_s from 26 to 18 $\Omega \text{ cm}^2$ (Figure S8 and Table S7) is found. These indicate that the devices with ZnO-C60 cathode do actually give a reduced R_s by promotion of electron conductivity at the interface and in the bulk of the cathode.

We also prepared PTB7-Th with different molecular weight (M_w) and polydispersity index (PDI) for device fabrication by use of different polymerization times. The corresponding $J-V$ curves of the devices fabricated therewith are given in Figure S9 (Supporting Information), and their characteristic parameters are listed in Table S8 (Supporting Information). For PTB7-Th with $M_w = 124000$ Da and PDI = 1.7, all of the parameters for the corresponding device are the highest among the PTB7-Th polymers we investigated. It seems that the polymer with narrow PDI and medium M_w gives better performance. This best PTB7-Th sample was used in the devices reported in the text.

In conclusion, we have presented the novel low-bandgap polymer PTB7-Th as a donor by combining the advantage of incorporating the 2-ethylhexyl-thienyl group into the BDT unit (BDT-T) to improve the coplanarity of the main chain (so that the absorption band can be extended to longer wavelengths by 25 nm along with enhanced absorption coefficient relative to PTB7) with the advantage of retaining the fluorine-substituted TT unit with the 2-ethylhexyl carboxylate group (F-TT) for a higher HOMO level. This PTB7-Th with PC₇₁BM as the acceptor is used as the active layer for i-PSCs. For effective collection of electrons, we present a simple and fast method for modification of ZnO as the cathode for i-PSCs by doping it with a fullerene derivative (PCBE-OH, 0.5 wt% of the ZnO precursor) to give a ZnO-C60 nanofilm (40 nm) on ITO as the cathode. This ZnO-C60 cathode provides dual functionalities for enhanced electron collection, including producing a fullerene-derivative-rich cathode surface and promotion of electron conductivity at the interface and bulk. For the device with ZnO-C60 as the cathode the PCE is improved for PTB7-Th:PC₇₁BM from 7.64% to 9.35%, for PTB7:PC₇₁BM from 6.65% to 8.21%, and for P3HT:ICBA from 5.26% to 6.60%, compared to that with ZnO cathode. The PCE of 9.35% is one of the best results that have been reported so far.

Experimental Section

The details of the synthesis of materials (monomers, polymers, PCBE-OH); purification procedures; fabrication of i-PSC; UPS, XPS, GIWAXS, and AFM measurements; and general instrumental measurements ($J-V$ characteristics, UV-vis spectra, EQEs, CV characteristics) are described in the Supporting Information.

Supporting Information

Supporting Information is available from the Wiley Online Library or from the author.

Acknowledgements

We thank the National Science Council for financial aid through project 101-2120-M-007-004 and Dr. Jey-Jau Lee for kind help with the grazing incidence wide-angle X-ray scattering (GIWAXS) of PTB7:PC₇₁BM and PTB7-Th:PC₇₁BM at beamline BL17A1 of the National Synchrotron Radiation Research Center (NSRRC, Taiwan).

Received: April 3, 2013

Revised: June 8, 2013

Published online: August 13, 2013

- [1] G. Yu, J. Gao, J. C. Hummelen, F. Wudl, A. J. Heeger, *Science* **1995**, 270, 1789.
- [2] W. Ma, C. Yang, X. Gong, K. Lee, A. J. Heeger, *Adv. Funct. Mater.* **2005**, 15, 1617.
- [3] F. C. Krebs, K. Norrman, *Prog. Photovoltaics: Res. Appl.* **2007**, 15, 697.
- [4] G. Li, C. W. Chu, V. Shrotriya, J. Huang, Y. Yang, *Appl. Phys. Lett.* **2006**, 88, 253503.
- [5] S. K. Hau, H. L. Yip, N. S. Baek, J. Zou, K. O'Malley, A. K. Y. Jen, *Appl. Phys. Lett.* **2008**, 92, 253301.
- [6] S. K. Hau, H. L. Yip, O. Acton, N. S. Baek, H. Ma, A. K. Y. Jen, *J. Mater. Chem.* **2008**, 18, 5113.
- [7] C.-H. Hsieh, Y.-J. Cheng, P.-J. Li, C.-H. Chen, M. Dubosc, R.-M. Liang, C.-S. Hsu, *J. Am. Chem. Soc.* **2010**, 132, 4887.
- [8] Y. Liang, D. Feng, Y. Wu, S.-T. Tsai, G. Li, C. Ray, L. Yu, *J. Am. Chem. Soc.* **2009**, 131, 7792.
- [9] H. Y. Chen, J. H. Hou, S. Q. Zhang, Y. Y. Liang, G. W. Yang, Y. Yang, L. P. Yu, Y. Wu, G. Li, *Nat. Photonics* **2009**, 3, 649.
- [10] Y. Liang, Z. Xu, J. Xia, S. T. Tsai, Y. Wu, G. Li, C. Ray, L. Yu, *Adv. Mater.* **2010**, 22, 1.
- [11] L. J. Huo, S. Q. Zhang, X. Guo, F. Xu, Y. F. Li, J. H. Hou, *Angew. Chem. Int. Ed.* **2011**, 50, 9697.
- [12] S.-H. Liao, Y.-L. Li, T.-Z. Jen, Y.-S. Cheng, S.-A. Chen, *J. Am. Chem. Soc.* **2012**, 134, 14271.
- [13] Z. He, C. Zhong, X. Huang, W.-Y. Wong, H. Wu, Li. Chen, S. Su, Y. Cao, *Adv. Mater.* **2011**, 23, 4636.
- [14] S. K. Hau, Y.-J. Cheng, H.-L. Yip, Y. Zhang, H. Ma, A. K.-Y. Jen, *ACS Appl. Mater. Interfaces* **2010**, 2, 1892.
- [15] Y.-J. Cheng, C.-H. Hsieh, Y. He, C.-S. Hsu, Y. Li, *J. Am. Chem. Soc.* **2010**, 132, 17381.
- [16] C.-Y. Chang, C.-E. Wu, S.-Y. Chen, C. Cui, Y.-J. Cheng, C.-S. Hsu, Y.-L. Wang, Y. Li, *Angew. Chem. Int. Ed.* **2011**, 50, 9386.
- [17] Z. He, C. Zhong, S. Su, M. Xu, H. Wu, Y. Cao, *Nat. Photonics* **2012**, 6, 591.
- [18] B. Walker, A. B. Tamayo, X.-D. Dang, P. Zalar, J. H. Seo, A. Garcia, M. Tantiwiwat, T.-Q. Nguyen, *Adv. Funct. Mater.* **2009**, 19, 3063.
- [19] H.-L. Yip, A. K. Y. Jen, *Energy Environ. Sci.* **2012**, 5, 5994.
- [20] J. Liu, S. Shao, G. Fang, B. Meng, Z. Xie, L. Wang, *Adv. Mater.* **2012**, 24, 2774.
- [21] X. Li, W. C. H. Choy, L. Huo, F. Xie, W. E. I. Sha, B. Ding, X. Guo, Y. Li, J. Hou, J. You, Y. Yang, *Adv. Mater.* **2012**, 24, 3046.
- [22] Y. Sun, J. H. Seo, C. J. Takacs, J. Seifter, A. J. Heeger, *Adv. Mater.* **2011**, 23, 1679.
- [23] S. T. Tan, X. W. Sun, Z. G. Yu, P. Wu, G. Q. Lo, *Appl. Phys. Lett.* **2007**, 91, 72101.
- [24] a) A. J. Maxwell, P. A. Brühwiler, A. Nilsson, N. Mårtensson, P. Rudolf, *Phys. Rev. B* **1994**, 49, 10717; b) M. P. Felicissimo, D. Jarzab, M. Gorgoi, M. Forster, U. Scherf, M. C. Scharber, S. Svensson, P. Rudolf, M. A. Loi, *J. Mater. Chem.* **2009**, 19, 4899.
- [25] D. Gao, J. Zhang, G. Yang, J. Zhang, Z. Shi, J. Qi, Z. Zhang, D. Xue, *J. Phys. Chem. C* **2010**, 114, 13477.
- [26] B. Yang, P. Feng, A. Kumar, R. S. Katiyar, M. Achermann, *J. Phys. D: Appl. Phys.* **2009**, 42, 195402.
- [27] a) O. Game, U. Singh, A. A. Gupta, A. Suryawanshi, A. Banpurkarb, S. Ogale, *J. Mater. Chem.* **2012**, 22, 17302; b) S.-M. Park, T. Ikegami, K. Ebihara, P.-K. Shin, *Appl. Surf. Sci.* **2006**, 253, 1522.
- [28] A. S. Riad, S. A. Mahmoud, A. A. Ibrahim, *Physica B* **2001**, 296, 319.
- [29] N. S. M. Sauki, M. H. R. A. Rahim, S. H. Herman, M. R. Mahmood, *2012 IEEE Symposium on Humanities, Science and Engineering Research (SHUSER)*, IEEE, Piscataway, NJ **2012**, DOI:10.1109/SHUSER.2012.6268824.